Biosensors and Bioelectronics 165 (2020) 112434

Contents lists available at ScienceDirect

Biosensors and Bioelectronics

journal homepage: http://www.elsevier.com/locate/bios

Evaluating the sensing performance of nanopore blockade sensors: A case study of prostate-specific antigen assay

Yanfang Wu *, Kyloon Chuah, J. Justin Gooding **

School of Chemistry, Australian Centre for NanoMedicine, Australian Research Council Centre of Excellence in Convergent Bio-Nano Science and Technology, The University of New South Wales, Sydney, New South Wales, 2052, Australia

ARTICLE INFO

Keywords:
Nanopore blockade sensor
Ultrasensitive biosensor
Nanopore sensing
Human plasma
Prostate-specific antigen
Single molecule detection

ABSTRACT

The detection principle of nanopore sensors relies on measuring changes in electrical signal as analyte molecules translocate through a nanoscale pore. There are two challenges with this experimental construct when using nanopores for quantitative sensing with low detection limits in complex samples. The first is getting the analyte to the nanopore in a reasonable time frame and the second is other species in the sample also translocating through the nanopore and generating erroneous signals. We have developed a nanopore blockade sensor that alleviates the limitations of diffusion-limited mass transport and non-specific signals. Antibody-modified magnetic nanoparticles are utilized to deliver analytes of interest extracted from sample to an array of antibody-modified nanopores under a controlled electromagnet, resulting in long-term nanopore blocking events due to the formation of sandwiched immunocomplexes. Herein, this study reports on understanding some of important parameters in determining the performance of nanopore blockade sensing system, where prostate-specific antigen (PSA) is used as a model analyte. We describe the characterization of nanopore blockade sensing of PSA by (1) tuning on/off the electromagnet, (2) varying nanopore number in a nanopore chip, and (3) deploying the sensor in human plasma. Results show that magnetophoresis effectively facilitates active delivery and selective sensing of PSA to the nanopore. Nanopore chips with a larger number of nanopores are shown to receive more nanopore blockades for a given concentration of analyte. Furthermore, identifiable blockade events accounted for successful detection of PSA in plasma, indicate the high specificity of the sensing system.

1. Introduction

Nanopore sensors can achieve single molecule resolution which have been exploited for a number of applications including next-generation sequencing (Shendure et al., 2017), tracking of reversible single-molecule covalent chemistry (Luchian et al., 2003; Qing et al., 2018; Shin et al., 2002), and revealing of transient intermediates and chemical reaction mechanism (Haugland et al., 2019; Lee and Bayley, 2015). It has been shown that even a single phosphorylation modification on a peptide can be identified by a nanopore-based sensor. Other than the utilization as single-molecule detectors, nanopores have also attracted attention as analytical sensors for quantitative analysis (Gooding and Gaus, 2016). From the earliest studies (Braha et al., 1997; Hladky and Haydon, 1970; Nikolelis et al., 1996; Walker et al., 1994), nanopores have been explored for stochastic sensing based on changes in electrical signal associated when analyte molecules translocate through the nanopore. Although significant advances have been achieved, two main challenges for the development of nanopore sensors as ultralow detection limit sensors still exist. The challenges are (1) long analysis times when utilized for quantification of analyte species in low abundance and (2) transient electrical signals that result from translocation events from both specific and non-specific molecules when dealing with complex biological samples (Wu et al., 2019).

The solution to these challenges could revolve around magnetic nanoparticles (MNPs). MNPs have been widely adopted as an effective solution to the development of ultrasensitive sensors (Gloag et al., 2019). So far, MNPs have been demonstrated to not only collect and separate analytes of interest from samples, but also be integrated as part of transduction element for generating signals. For instance, the "dispersible electrodes" concept (Chuah et al., 2012; Goon et al., 2010a; Lai et al., 2012; Tavallaie et al., 2018) described by our group has been shown to significantly reduce response time and lower detection limits

* Corresponding author.
** Corresponding author.
E-mail addresses: yanfang.wu@unsw.edu.au (Y. Wu), justin.gooding@unsw.edu.au (J.J. Gooding).

https://doi.org/10.1016/j.bios.2020.112434
Received 19 April 2020; Received in revised form 3 July 2020; Accepted 6 July 2020
Available online 8 July 2020

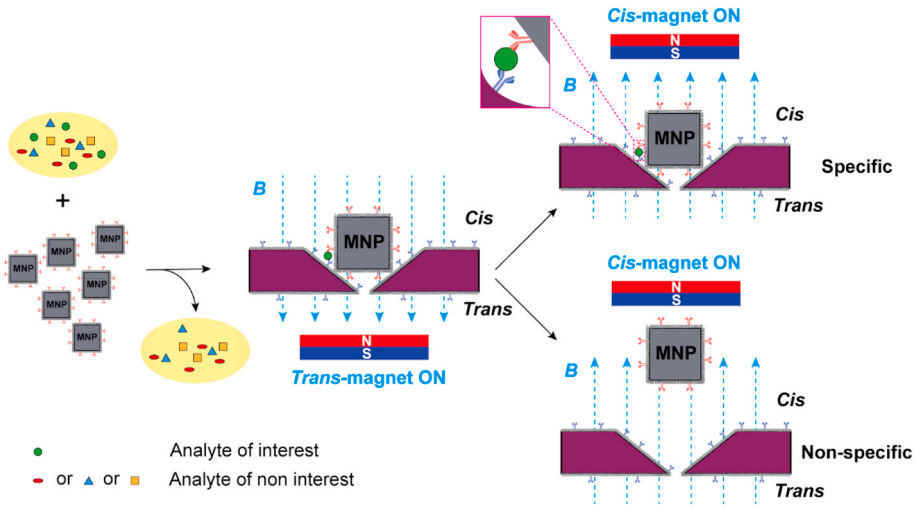

Scheme 1. Schematic of the workflow of nanopore blockade sensing. After collecting target analyte (i.e., prostate-specific antigen, PSA) from sample solution, anti-PSA antibody modified MNPs (abbreviated as (anti-PSA)-MNPs) are magnetically separated, and washed several times to remove non-specifically adsorbed molecules followed by performing magnetic analyte shuttling to differentiate specific versus non-specific blocking events for bioanalytical sensing of PSA.

by more than 2500-fold, compared to the response from a conventional planar surface-based sensor (Chuah et al., 2012). The key advantage of MNPs with the dispersible electrode concept is that they, not only reduce response time by bringing the analyte more rapidly to the sensing surface, but also collect more of the analyte such that the sensitivity of the sensor is greater (Goon et al., 2010a). These same features could be used for nanopore sensing, but to date MNPs have only gained limited attention in nanopore sensing. MNPs have been utilized to preconcentrate analyte molecules such as microRNA (Wang et al., 2019; Wanunu et al., 2010) and protein (Li et al., 2015; Tang et al., 2020) from a biological sample followed by releasing their cargo into a measurement solution for quantitation. Such a strategy results in lowered detection limits. Integration of MNPs into the transduction mechanism of nanopore sensing is only now beginning.

Recently, we demonstrated the proof-of-concept work of nanopore blockade sensors where MNPs not only were used to selectively capture a target protein (prostate-specific antigen, PSA) but also were integrated with a solid-state nanopore array as part of the ionic current readout mechanism (Chuah et al., 2019). This was achieved using anti-PSA antibody modified MNPs ((anti-PSA)-MNPs) that irreversibly blocked the nanopore if the analyte was captured; thus changing the sensing paradigm from stochastic translocation to blocking the nanopore in a more deterministic fashion. The (anti-PSA)-MNPs served as an effective means to facilitate the mass transport of target analyte to an array of nanopores, thus enabling sensitive detection of single analyte molecules in parallel from high fidelity ionic current signals. This approach also provided the ability to distinguish specific versus non-specific molecules by reversing the applied magnetic field (Wu et al., 2020). The nanopore blockade sensors provided rapid, sensitive, and selective detection of protein species with sub-fM detection limits.

In a typical nanopore blockade sensing experiment (Scheme 1), taking the detection of PSA at ultralow concentration levels as an example, (anti-PSA)-MNPs are mixed with a sample solution to capture PSA molecules. Because of the excess of (anti-PSA)-MNPs over PSA molecules, Poisson statistics comes into effect such that a single (anti-PSA)-MNP carries one PSA molecule at most. The (anti-PSA)-MNPs are then collected by a magnet followed by rinsing to remove non-specifically adsorbed molecules before adding them to electrolyte solution in the *cis*-side of the chamber of a flow cell for ionic current measurement. Thereafter, (anti-PSA)-MNPs are brought to an array of anti-PSA modified nanopores using a *trans*-magnet. The (anti-PSA)-MNPs in the *cis*-side compartment can block the nanopores but not translocate through the nanopore due to the nanoparticle size being engineered to be slightly larger than the nanopore diameter of the bottom opening (*trans*). An important feature of the nanopore blockade sensor is the capability of magnetic field reversal. Only when the (anti-PSA)-MNP in a blocked nanopore carries a PSA molecule, which then also binds to anti-PSA antibody on the nanopore surface, does the single molecule immunocomplex lead to the detection of an irreversible nanopore blockade event (no unblocking) under a reversed magnetic field. In contrast, when a nanopore is non-specifically blocked by a (anti-PSA)-MNP that has no captured PSA, the (anti-PSA)-MNP is removed from the nanopore under the application of the *cis*-magnet. This sensing paradigm enhances the sensor specificity and enables the selective detection of PSA from complex biological samples.

The purpose of the current study is to build on this initial work and further understand the capability behind the nanopore blockade sensor for highly sensitive and selective detection of PSA. Three key factors that could significantly affect the sensing performance are evaluated. Firstly, the coupling of controllable electromagnets with (anti-PSA)-MNPs to obtain magnetic guidance and facilitated transport of PSA molecules for nanopore blockade sensing was studied through the comparison of ionic current recordings in the presence and absence of electromagnets. Next, the effect of the number of nanopores in a solid-state membrane on the detection of 0.8 fM PSA was investigated. A comparison was thereby made regarding the mean values of nanopore blockades obtained from two kinds of nanopore chips containing 3×3 and 4×4 nanopore arrays, respectively. Lastly, a demonstration of the detection of PSA directly from human plasma by nanopore blockade sensors was explored as well.

2. Experimental section

Details about chemicals, reagents, apparatus, and experimental methods can be found in Supplementary Information.

3. Results and discussion

3.1. Development of nanopore blockade sensors for the detection of PSA

A nanopore blockade sensor includes two key components – one is the solid-state nanopores and the other is the MNPs. Solid-state nanopores were produced in free-standing silicon nitride (SiN) membranes. As shown in Fig. 1a, commercial 105-μm-thick Si(100) wafers sandwiched with SiN film on both sides were employed as the starting material and a total of 88 nanopore chips could be obtained from a single 4 inch wafer (see Fig. S1 for the illustration of the fabrication process). An

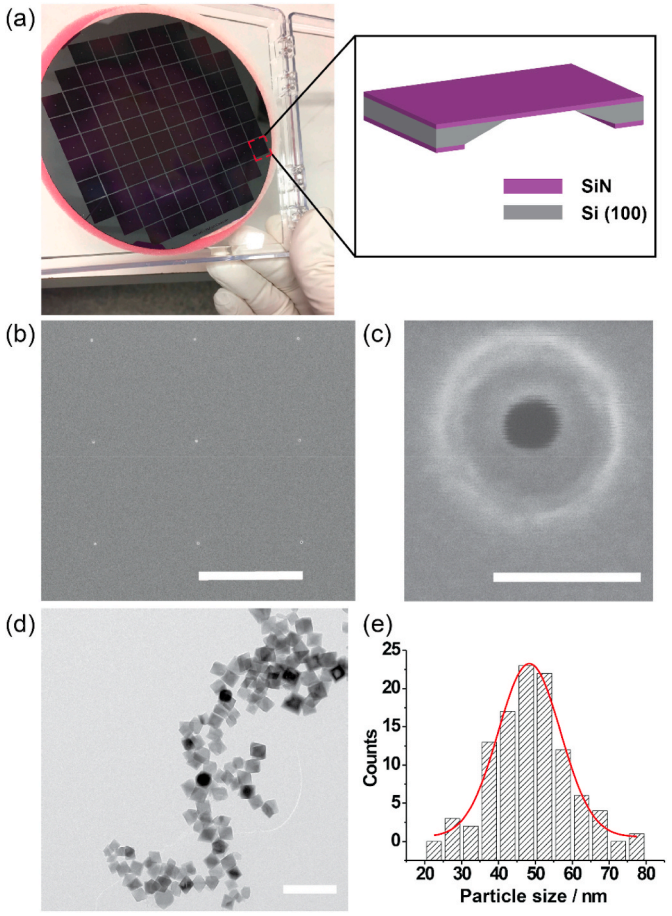

Fig. 1. (a) A photograph of a 4-inch wafer containing an 88-chip pattern. The illustration in the right inset depicts a nanopore chip with a free-standing silicon nitride (SiN) membrane. (b) Scanning electron microscopy (SEM) image of 3 × 3 nanopore array. Scale bar, 5 μm. (c) Enlarged magnification of SEM image of a typical nanopore in SiN membrane. Scale bar, 100 nm. (d) Transmission electron microscopy image of cubic magnetic nanoparticles (MNPs). Scale bar, 200 nm. (e) Size distribution of the synthesized polyethyleneimine coated MNPs. Gaussian fit (red line) yields an average nanoparticle size of (48.3 ± 9.9) nm (Number of MNPs measured, N = 103). (For interpretation of the references to colour in this figure legend, the reader is referred to the Web version of this article.)

illustration of a nanopore chip is given to the right inset of Fig. 1a. The SiN surface, after rinsing with acetone and isopropanol, was coated with a layer of ZEP520A electron beam resist. The resultant resist film was measured to be (427 ± 9) nm thick under the applied experimental conditions (see Fig. S2 for the surface profile of a ZEP520A resist coated SiN surface). The change in surface hydrophilicity before and after coating with ZEP520A resist was characterized by water contact angle measurement. The contact angle was measured to be $(35.6 \pm 2.4)^{o}$ on oxygen plasma cleaned SiN surface, whereas it increased to $(73.8 \pm 2.5)^{o}$ on ZEP520A coated SiN surface; a significant change in water contact angle was observed (see the inset pictures in Fig. S2). Next, arrays of 15 × 15 dots were produced in the resist coated chip by exposing to electron beam with controlled exposure doses on each array followed by developing exposed samples in *N*-amyl acetate and rinsing with methyl isobutyl ketone. The resultant arrays of dots in the resist film, appeared as green dots under a dark-field optical microscopy, showed that the dot size increased with the dose of the applied electron beam (see Fig. S3 for the dark-field optical microscope image). Dry reactive ion etching was then performed to transfer the as drawn pattern from the resist film to the underlying SiN surface. As such, nanoscale pores with a control over nanopore diameter and position in SiN membranes can be reliably fabricated. Fig. S4 provides several representative scanning electron microscopy (SEM) images of SiN nanopores of different diameters.

In this study, we used nanopore chips with a 3 × 3 nanopore array with a spacing distance between adjacent nanopores of 5 μm. Fig. 1b presents a SEM image of such 3 × 3 nanopore array in SiN membrane. Our previous calculations (Chuah et al., 2019) suggested that this spacing ensures individual nanopores are sufficiently separated such that local electric fields from one nanopore do not interfere with adjacent nanopores. Therefore, a 5 μm spacing distance was chosen for further investigations hereafter. Furthermore, the fabricated nanopores presented a truncated conical shape. A typical top view image of a nanopore is presented in Fig. 1c, which shows the respective diameters of 30 nm for bottom opening and 100 nm for top opening. Meanwhile, cubic MNPs coated with positively charged polyethyleneimine were obtained following a previously reported method (Goon et al., 2010b) (Fig. 1d). Statistical analysis from the transmission electron microscopy image indicates the approximate size of the MNP was (48.3 ± 9.9) nm in length (Fig. 1e). It is worth noting that the relative dimensions of nanopores and MNPs were deliberately designed to ensure that the nanoparticle size was slightly larger than the nanopore diameter of the bottom opening. As a result, the MNP could not translocate through the nanopore, but instead block the nanopore. In addition to this, the space confined by a nanopore can only accommodate a single MNP and thereby electrically detected discrete nanopore blocking events can be attributed to the blocking of nanopores by single MNPs in parallel.

Nanopore blockade sensors were developed for the detection of PSA, selected here as the model protein analyte. Hence, the respective surfaces on nanopores and MNPs were modified with two anti-PSA antibodies that can bind to the PSA molecule at different sites (see Figs. S5 and S6 for the schematics of surface modification processes).

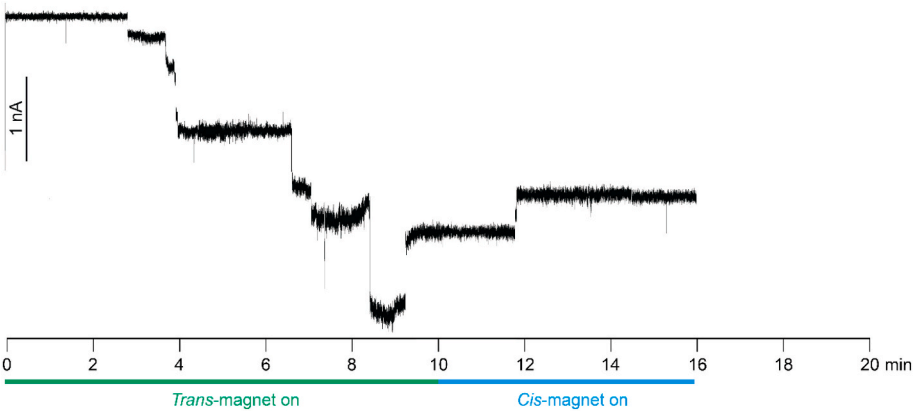

Fig. 2. Current-time trace from a nanopore chip containing an array of 3 × 3 nanopores modified with anti-PSA antibodies for differentiating specific and non-specific blockade events. The (anti-PSA)-MNPs (1.87×10^{9} nanoparticles) were mixed with a solution of 4 fM PSA, separated magnetically and washed several times before adding to 100 mM KCl solution. The applied magnetic field included 10 min for a *trans*-magnet and subsequently ~6 min for a *cis*-magnet. Potential bias, 100 mV; electrolyte solution, 100 mM KCl (10 mM Tris-HCl, 0.05% Tween-20, pH 7.4).

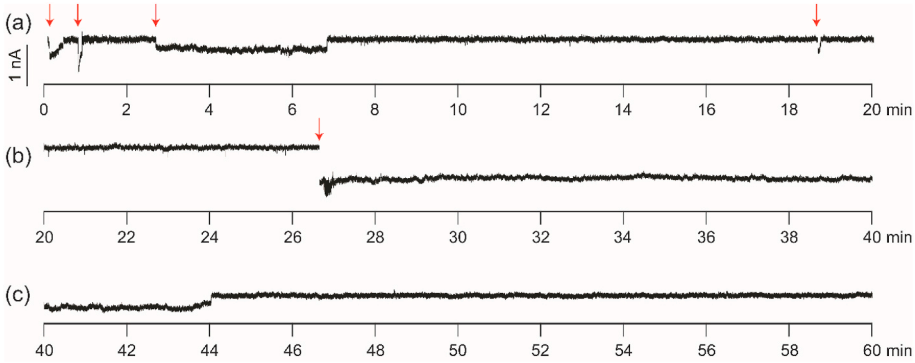

Fig. 3. Current-time traces from a nanopore chip containing an array of 3 × 3 nanopores modified with anti-PSA antibodies. Ionic current recordings in the time frame of (a) 0–20 min, (b) 20–40 min, and (c) 40–60 min are provided. The (anti-PSA)-MNPs were mixed with a solution of 588.2 fM PSA, separated magnetically and washed several times before adding to 100 mM KCl solution. Potential bias, 100 mV; electrolyte solution, 100 mM KCl (10 mM Tris-HCl, 0.05% Tween-20, pH 7.4).

3.2. The effect of magnetophoresis on nanopore blockade sensing

Experiments were carried out to understand the contribution by magnetophoresis to nanopore blockade sensing system. Firstly, the response of (anti-PSA)-MNPs to an external magnetic field was demonstrated to show the facilitated transport of (anti-PSA)-MNPs to the array of nanopores. Fig. 2 provides an example of current-time trace from a nanopore chip containing 3 × 3 nanopore array. The (anti-PSA)-MNPs were treated with a solution of 4 fM PSA before ionic current recording. As the nanopores are similar in size, each nanopore blockade would cause a similar amount of current reduction. Hence, after switching on the *trans*-magnet, six sequential nanopore blocking events were observed associated with a stepwise drop in the time trace of ionic current, which enabled the counting of nanopore blocking events (Fig. 2). An average frequency of blocking events of 4.8 counts per 10 min under the *trans*-magnet was obtained from 43 independent ionic current measurements. This clearly indicates that using a magnetophoretic force can dramatically enhance the transport of (anti-PSA)-MNPs and active delivery of PSA molecules bound on nanoparticles to the sensing points. In addition, the reversal of magnetic field direction offers the opportunity to selectively detect PSA molecules enabled by the (anti-PSA)-MNPs sitting inside the nanopores. Under the *cis*-magnet, two (anti-PSA)-MNPs were ejected from the nanopores, whereas the remaining four nanopore blocking events were found to be specific due to the specific immunobinding of PSA by anti-PSA antibodies on nanopores. The long-term nanopore blockade events under the *cis*-magnet, indicate that the immunobinding affinity is strong enough to withstand the magnetic force. Taken together, the combination of controllable magnetic fields and (anti-PSA)-MNPs demonstrates the rapid delivery of analyte molecules and specific differentiation in nanopore blockade sensing.

In the absence of a magnetic field, ionic current was recorded for 1 h after adding 1.87×10^9 (anti-PSA)-MNPs to 100 mM KCl solution in the *cis*-side compartment. In the first 20 min, four (anti-PSA)-MNPs came close to the array of 3 × 3 nanopores but escaped without blocking the nanopore as demonstrated by the rapid reduction in ionic current followed by a recovery back to its original current level (Fig. 3a). Subsequently, a dramatic drop in current was observed in ~27^{th} min which resulted from the blocking of a nanopore by one (anti-PSA)-MNP. The blockage greatly limited the ionic flux through the nanopore and hence the current dropped (Fig. 3b). No further nanoparticle blockade events were detected. In ~44^{th} min, the recovery of the conductance suggested that the above blocked nanopore was unblocked and the nanoparticle diffused away from the nanopore after a residence time of about 14 min (Fig. 3c). The frequency of blocking events was calculated to be 0.8 counts per 10 min in the absence of a magnetic field, as distinct from 4.8 per 10 min with a magnetic field applied. These results clearly indicate that it is inefficient for (anti-PSA)-MNPs to come close to nanopores and block the pore in a passive transport way governed by Brownian motion and electrophoresis.

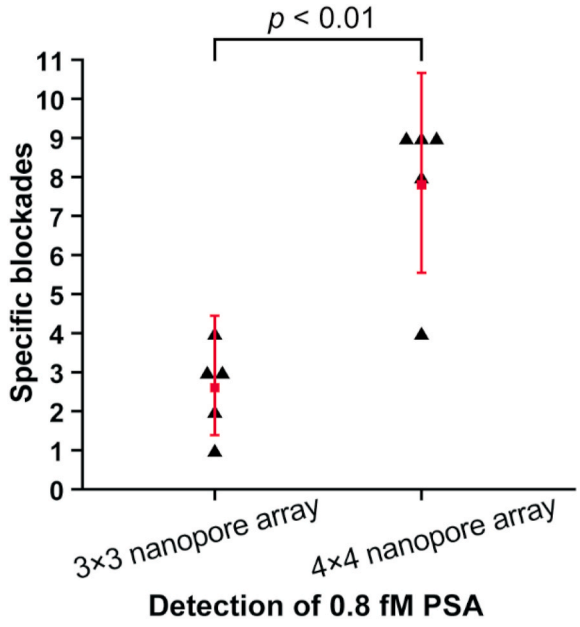

Fig. 4. Comparison of the mean value of specific nanopore blockades determined with two respective nanopore chips containing 3 × 3 and 4 × 4 nanopores in the presence of 0.8 fM PSA. Each data point was obtained from an independent nanopore chip. Mean values as well as 95% confidence intervals (calculated by the exact method for Poisson means) are presented. Numbers of nanopore blockades were determined after 4 times of magnet switching cycle. Each cycle is comprised of 10 min for a *trans*-magnet and 5 min for a *cis*-magnet. The number of (anti-PSA)-MNPs employed was ~1.87×10^9. Based on Poisson statistics, individual specific nanopore blockade events were attributed to the formation of single immunocomplexes as a single (anti-PSA)-MNP carries one PSA molecule at most under the experimental conditions. A two-tailed z-test (of square root transform version) was used to test the difference for the two Poisson means.

3.3. The effect of nanopore number on nanopore blockade sensing

Nanopore blockade sensors correlate the number of specific nanopore blockades, caused by (anti-PSA)-MNPs after treating with samples, with PSA concentration level in the sample. Thereby, to understand the effect of the number of nanopores on the sensing performance of nanopore blockade sensors, two kinds of nanopore chips containing an array of 3 × 3 and 4 × 4 nanopores respectively were employed.

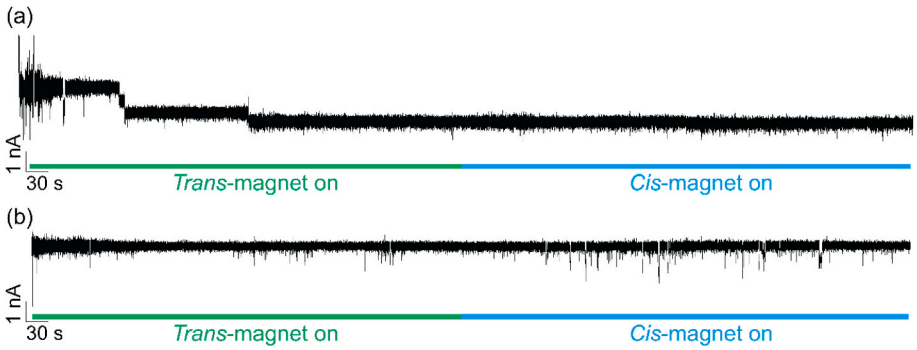

Fig. 5. Current-time traces from nanopore chips containing 3 × 3 nanopore array measured directly from plasma (a) with and (b) without adding 1.87 × 10^9 (anti-PSA)-MNPs. The *cis*- and *trans*-side chambers of the flow cell were filled with plasma and 100 mM KCl solution (10 mM Tris-HCl, 0.05% Tween-20, pH 7.4), respectively. Potential bias: 100 mV; low-pass-filtered at 1 kHz and sampled at 250 kHz. The applied magnetic field included 10 min for a *trans*-magnet and subsequently ~10 min for a *cis*-magnet.

Current-time traces were recorded under a potential bias of 100 mV and numbers of specific nanopore blockades were taken after 4 cycles of magnet switching. Previous work (Chuah et al., 2019) has shown that there is a positive correlation between the average value of specific nanopore blockades and the PSA concentration in the sample, which can be used for quantitative analysis. As shown in Fig. 4, the mean value of specific nanopore blockades corresponding to 0.8 fM PSA was 2.6 counts for 3 × 3 nanopore array, whereas it increased to 7.8 counts for 4 × 4 nanopore array. The free-standing SiN membrane has a surface size of about 240 × 240 μm^2, which is much greater than a nanopore that has a ~100 nm top orifice (*cis*). The more nanopores presented in the membrane, the larger area they cover on the chip. Therefore, it is anticipated that when working with a chip of a larger number of nanopores, more nanoparticles would enter the nanopores under the *trans*-magnet. Hence, the nanopore blockade sensors would be more sensitive and have a lowered detection limit. Furthermore, using nanopore chips with a larger array of nanopores could be expected to extend the upper end of the dynamic range and thus yield the establishment of a wider dynamic range to different analyte concentrations. Additionally, analyte quantitation accuracy would then be improved by using such nanopore sensor with a higher sensitivity to ultralow concentrations and a wider dynamic range. Therefore, it may be possible that by scaling up the number of nanopores in a nanopore chip, one may improve the sensor performance including wider response ranges, lower detection limits and higher accuracy of measurements will be achieved. The limitation to how many nanopores can be used in an array however will be determined by the magnitude of the change in current during a single nanoparticle blockade and the magnitude of the electronic noise in the signal.

3.4. Direct nanopore blockade sensing of PSA in human plasma

Conventional nanopore sensors possess the specificity challenge as the sensors acquire through-pore current signals from both specific and non-specific molecules. To demonstrate the specificity for nanopore blockade sensors against non-specific molecules and its excellent tolerance to complex biological *milieu*, ionic currents were recorded directly in human plasma samples containing ~21 pM PSA. This is in contrast to nanoporous membrane integrated in front of a single-nanopore chip where serum was filtered by the integrated membrane under an applied pressure, which helped to limit the interference from non-specific molecules and facilitate the direct detection of target biomarker in serum (Lin et al., 2017). The (anti-PSA)-MNPs were added to plasma and the mixture was kept for 1 h. Afterwards, the above mixture was added to the *cis*-side chamber while degassed KCl solution was introduced to the *trans*-side chamber. Fig. 5a clearly presents sequential blocking events after switching on the *trans*-magnet. However, no unblocking event was observed under the *cis*-magnet. This suggests the successful detection of PSA molecules in plasma as indicated by the specific nanopore blockades. Furthermore, a control experiment was performed when plasma and KCl solution were added to the *cis*- and *trans*-side chambers, respectively. The current-time trace shows no blocking events (Fig. 5b), which confirmed that the irreversible blockade events in Fig. 5a were due to the (anti-PSA)-MNPs with captured PSA molecules. In addition, the analysis of the current noise in the power spectrum indicates that the noise in the low-frequency (≤100 Hz) range was 10 times noisier when plasma was presented in the *cis*-side chamber, compared to that when both *cis*- and *trans*-side chambers were filled with KCl solution (see Fig. S7 for the power spectral density noise analysis). Nonetheless, distinguishable specific nanopore blockade events were observed at plasma (Fig. 5a). These results are significant as our previous work (Chuah et al., 2019) has shown that PSA molecules can be captured and isolated by (anti-PSA)-MNPs from human whole blood samples, then sensing and quantification were performed in a measurement solution. Here, the direct nanopore blockade sensing of PSA in human plasma was successfully demonstrated even though PSA molecules were outnumbered by many more non-specific proteins and molecules in the plasma and their inevitable adsorption occurred on the sensing interface. Taken together, these results indicate that nanopore blockade sensors present the potential to directly assay PSA molecules from clinical samples without requiring time-consuming sample pre-treatment.

4. Conclusions

Herein, this study reports the characterization and determination studies of nanopore blockade sensing system. Useful insights were obtained after experimentally investigating three important factors that could influence the sensing and quantification of PSA. The introduction of magnetophoresis demonstrated to be effective to alleviate the slow mass transport limited by diffusion and stochastic detection. The combination of magnetic fields and MNPs significantly reduced analysis time and facilitated (anti-PSA)-MNPs with captured PSA to find the location of the nanopores. It was shown that the more nanopores in a nanopore chip, the more specific nanopore blockades for a give concentration of analyte. This points to a practical approach for nanopore blockade sensors to further lower detection limits, extend the dynamic range and improve detection accuracy through scaling up nanopore number in a nanopore chip. Furthermore, unambiguously detecting specific nanopore blockades in human plasma was successfully demonstrated, indicating that nanopore blockade sensors may bear the potential to be used for on-site clinical diagnosis because of the elimination of sample preparation. These findings are expected to be useful to further the development of nanopore blockade sensors in ultralow detection limit biosensing applications from complex biological *milieu*.

One potential concern is if the capture surface chemistry, i.e., anti-PSA antibody in this study is immobilized everywhere on the chip surface, some of the nanoparticles bound with PSA may be lost because they may bind to those antibodies on the *cis* membrane which is much wider than nanopore surfaces. This would decrease the number of specific nanopore blockades for analyte quantification. A solution to this is to develop nanopore chips with spatially specific surface functionalization on nanopore interiors and exteriors to confine specific recognition

occurred only in nanopores which we are currently working on. The challenge is that one cannot keep increasing the number of nanopores in a chip. For nanopore sensing based on electrical current measurement, the change in signal-to-noise ratio to detect a single nanoparticle blockade above the background signal would be a trade-off. Solutions to this latter challenge (Huang et al., 2015) have already been demonstrated with nanopore arrays with an optical readout which could also be employed in conjunction with the nanopore blockade sensor reported herein.

Declaration of competing interest

The authors declare that they have no known competing financial interests or personal relationships that could have appeared to influence the work reported in this paper.

CRediT authorship contribution statement

Yanfang Wu: Conceptualization, Methodology, Formal analysis, Investigation, Data curation, Writing - original draft, Writing - review & editing, Visualization, Supervision, Project administration. **Kyloon Chuah:** Writing - review & editing. **J. Justin Gooding:** Conceptualization, Resources, Writing - review & editing, Supervision, Project administration, Funding acquisition.

Acknowledgments

This research was supported by the Australian Research Council through the ARC Centre of Excellence in Convergent Bio-Nano Science and Technology (CE140100036) and an ARC Australian Laureate Fellowship (FL150100060). The fabrication work was performed in part at the NSW Node of the Australian National Fabrication Facility (ANFF).

Appendix A. Supplementary data

Supplementary data to this article can be found online at https://doi.org/10.1016/j.bios.2020.112434.

References

Braha, O., Walker, B., Cheley, S., Kasianowicz, J.J., Song, L., Gouaux, J.E., Bayley, H., 1997. Chem. Biol. 4, 497–505.
Chuah, K., Lai, L.M.H., Goon, I.Y., Parker, S.G., Amal, R., Gooding, J.J., 2012. Chem. Commun. 48, 3503–3505.
Chuah, K., Wu, Y., Vivekchand, S.R.C., Gaus, K., Reece, P.J., Micolich, A.P., Gooding, J. J., 2019. Nat. Commun. 10, 2109.
Gloag, L., Mehdipour, M., Chen, D., Tilley, R.D., Gooding, J.J., 2019. Adv. Mater. 31, 1904385.
Gooding, J.J., Gaus, K., 2016. Angew. Chem. Int. Ed. 55, 11354–11366.
Goon, I.Y., Lai, L.M.H., Lim, M., Amal, R., Gooding, J.J., 2010a. Chem. Commun. 46, 8821–8823.
Goon, I.Y., Zhang, C., Lim, M., Gooding, J.J., Amal, R., 2010b. Langmuir 26, 12247–12252.
Haugland, M.M., Borsley, S., Cairns-Gibson, D.F., Elmi, A., Cockroft, S.L., 2019. ACS Nano 13, 4101–4110.
Hladky, S.B., Haydon, D.A., 1970. Nature 225, 451–453.
Huang, S., Romero-Ruiz, M., Castell, O.K., Bayley, H., Wallace, M.I., 2015. Nat. Nanotechnol. 10, 986–991.
Lai, L.M.H., Goon, I.Y., Chuah, K., Lim, M., Braet, F., Amal, R., Gooding, J.J., 2012. Angew. Chem. Int. Ed. 51, 6456–6459.
Lee, J., Bayley, H., 2015. Proc. Natl. Acad. Sci. Unit. States Am. 112, 13768–13773.
Li, T., Liu, L., Li, Y., Xie, J., Wu, H.-C., 2015. Angew. Chem. Int. Ed. 54, 7568–7571.
Lin, Y., Ying, Y.-L., Shi, X., Liu, S.-C., Long, Y.-T., 2017. Chem. Commun. 53, 11564–11567.
Luchian, T., Shin, S.-H., Bayley, H., 2003. Angew. Chem. Int. Ed. 42, 3766–3771.
Nikolelis, D.P., Siontorou, C.G., Krull, U.J., Katrivanos, P.L., 1996. Anal. Chem. 68, 1735–1741.
Qing, Y., Ionescu, S.A., Pulcu, G.S., Bayley, H., 2018. Science 361, 908–912.
Shendure, J., Balasubramanian, S., Church, G.M., Gilbert, W., Rogers, J., Schloss, J.A., Waterston, R.H., 2017. Nature 550, 345–353.
Shin, S.-H., Luchian, T., Cheley, S., Braha, O., Bayley, H., 2002. Angew. Chem. Int. Ed. 41, 3707–3709.
Tang, H., Wang, H., Yang, C., Zhao, D., Qian, Y., Li, Y., 2020. Anal. Chem. 92, 3042–3049.
Tavallaie, R., McCarroll, J., Le Grand, M., Ariotti, N., Schuhmann, W., Bakker, E., Tilley, R.D., Hibbert, D.B., Kavallaris, M., Gooding, J.J., 2018. Nat. Nanotechnol. 13, 1066–1071.
Walker, B., Kasianowicz, J., Krishnasastry, M., Bayley, H., 1994. Protein Eng. Des. Sel. 7, 655–662.
Wang, H., Tang, H., Yang, C., Li, Y., 2019. Anal. Chem. 91, 7965–7970.
Wanunu, M., Dadosh, T., Ray, V., Jin, J., McReynolds, L., Drndić, M., 2010. Nat. Nanotechnol. 5, 807–814.
Wu, Y., Bennett, D., Tilley, R.D., Gooding, J.J., 2020. Adv. Mater. 32, 1904339.
Wu, Y., Tilley, R.D., Gooding, J.J., 2019. J. Am. Chem. Soc. 141, 1162–1170.